

Solid-State Reactions

International Edition: DOI: 10.1002/anie.201813120
German Edition: DOI: 10.1002/ange.201813120Pressure-Induced Diels–Alder Reactions in C₆H₆-C₆F₆ Cocrystal towards Graphane Structure

Yajie Wang, Xiao Dong, Xingyu Tang, Haiyan Zheng,* Kuo Li,* Xiaohuan Lin, Leiming Fang, Guang'ai Sun, Xiping Chen, Lei Xie, Craig L. Bull, Nicholas P. Funnell, Takanori Hattori, Asami Sano-Furukawa, Jihua Chen, Dale K. Hensley, George D. Cody, Yang Ren, Hyun Hwi Lee, and Ho-kwang Mao

HPSTAR
697-2019

Abstract: Pressure-induced polymerization (PIP) of aromatics is a novel method for constructing sp³-carbon frameworks, and nanowires with diamond-like structures were synthesized by compressing benzene and its derivatives. Here by compressing a benzene-hexafluorobenzene cocrystal (CHCF), H-F-substituted graphane with a layered structure in the PIP product was identified. Based on the crystal structure determined from the *in situ* neutron diffraction and the intermediate products identified by gas chromatography-mass spectrum, we found that at 20 GPa CHCF forms tilted columns with benzene and hexafluorobenzene stacked alternatively, and leads to a [4+2] polymer, which then transforms to short-range ordered H-F-substituted graphane. The reaction process involves [4+2] Diels–Alder, retro-Diels–Alder, and 1-1' coupling reactions, and the former is the key reaction in the PIP. These studies confirm the elemental reactions of PIP of CHCF for the first time, and provide insight into the PIP of aromatics.

sp³-hybridized carbon-based materials have gained constant attention because of their outstanding mechanical and optical properties.^[1] However, their types are very limited compared to the diversity of the carbon-based molecules. Applying extreme pressure to unsaturated molecules, such as aromatics, is proven to be effective in constructing sp³-hybridized carbon materials.^[2] It is well known that benzene polymerizes into amorphous hydrogenated carbon under high pressure,^[3] and with anisotropic stress, a well-ordered single-crystal carbon

nanowire was reported, which is recognized as an ultra-thin sp³-carbon nanowire.^[2a,b] Similarly, single-crystal carbon nitride was synthesized by compressing pyridine slowly.^[2c] Recently, it was reported that aniline forms diamond-like polyaniline under external pressure and the hydrogen bond between the NH₂ groups is believed to be responsible for better crystallinity.^[2d] Besides the one-dimensional structure, the graphane structure was also obtained by compressing the aromatics under high-pressure and high-temperature conditions.^[4]

The reaction mechanism of these pressure-induced polymerizations (PIPs) was explored from various perspectives. Various possible connections between benzene molecules were theoretically proposed, and the energies of the formed dimers were examined to evaluate the corresponding reactions.^[5,6] Experimentally, a possible reaction route including a [4+2] cycloaddition reaction followed by an intramolecular “zipper” cascade reaction, was proposed according to the π–π stacking of the benzene molecules and the structural model of the product.^[2a] All of these reports suggest the reaction starts from the bonding between the π–π stacked aromatics. However, more experimental work is needed to understand the elemental reactions in the PIP process and its relation to the π–π stacking.

The C₆H₆-C₆F₆ 1:1 cocrystal (abbreviated as CHCF hereafter) provides an appropriate π–π stacking model because of the strong electrostatic attraction between C₆H₆ and C₆F₆.

[*] Dr. Y. Wang, Dr. X. Dong, Dr. X. Tang, Dr. H. Zheng, Dr. K. Li, Dr. X. Lin, Dr. H.-k. Mao
Center for High Pressure Science and Technology Advanced Research
Beijing, 100094 (P. R. China)
E-mail: zhenghy@hpstar.ac.cn
likuo@hpstar.ac.cn

Dr. L. Fang, Dr. G.'a. Sun, Dr. X. Chen, Dr. L. Xie
Key Laboratory of Neutron Physics and Institute of Nuclear Physics
and Chemistry, China Academy of Engineering Physics
Mianyang, 621999 (P. R. China)

Dr. C. L. Bull, Dr. N. P. Funnell
ISIS Neutron and Muon Facility, Rutherford Appleton Laboratory,
Chilton, Didcot, Oxon, OX11 0QX (UK)

Dr. T. Hattori, Dr. A. Sano-Furukawa
J-PARC Center, Japan Atomic Energy Agency
Tokai, Ibaraki 319-1195 (Japan)

Dr. J. Chen, Dr. D. K. Hensley
Center for Nanophase Materials Sciences, Oak Ridge National
Laboratory, Oak Ridge, TN 37831 (USA)

Dr. G. D. Cody, Dr. H.-k. Mao
Geophysical Lab, Carnegie Institution of Washington
5251 Broad Branch Road, NW, Washington, DC 20015 (USA)

Dr. Y. Ren
Advanced Photon Source, Argonne National Laboratory
Lemont, IL 60439 (USA)

Dr. H. H. Lee
Pohang Accelerator Laboratory, POSTECH
Pohang 790-784 (Republic of Korea)

Dr. X. Dong
Key Laboratory of Weak-Light Nonlinear Photonics, School of
Physics, Nankai University, Tianjin 300071 (China)

Supporting information and the ORCID identification number(s) for the author(s) of this article can be found under:
<https://doi.org/10.1002/anie.201813120>

The alternate stacking of C_6H_6 and C_6F_6 can be recognized as half of the benzene molecules being replaced by hexafluorobenzene, and thus provides a tracer during the reaction. Herein we report the PIP of CHCF and its reaction mechanism under applied pressure. The product of PIP contains a hydrogenated fluorinated graphane-like structure. Diels–Alder, retro-Diels–Alder, and 1–1' coupling reactions were identified during this process and the former is the key elemental reaction leading to the polymerized material. We describe the PIP route of the aromatic molecules systematically, which provides an alternative method for constructing substituted graphane with atomic-level uniformity.

CHCF forms rhombohedral crystals (phase I, $R\bar{3}m$) around room temperature and experiences three phase transitions to form phases II ($I2/m$), III ($P\bar{1}$), and IV ($P2_1/a$) at low temperature and ambient pressure.^[7] In all the phases, C_6H_6 and C_6F_6 are alternately stacked.^[7] Under high pressure, phases V ($P2_1/c$), VI, VII, and VIII were identified and PIP was observed at about 20 GPa after phase VIII.^[8] Combining in situ synchrotron X-ray diffraction (XRD; see Figure S1 in the Supporting Information), constant wavelength and time of flight (TOF) neutron diffraction under high pressure (see Figure S2), we determined the structures of phase VI, VII, and VIII ab initio (see Figure S3), including the atomic positions using Rietveld refinement (see Table S1). The C_6H_6 and C_6F_6 molecules are still alternately stacked to form columns in these phases. However, the columns are tilted significantly, and are quite different from those under low temperature. To understand the crystal structure at reaction pressure threshold more precisely, we further optimized the structure of phase VIII by using density-functional theory (DFT) calculations based on the experimental result at 20 GPa, as shown in Figure 1. The stacked aromatic rings are progressively tilted away from the previous column axis (c -axis), and form closed packed layers on the (102) plane. Every aromatic ring is curved and stacked on the interstitial site of three rings of the neighboring layer, with two of the three rings being of the same type. Along the [001] direction, the nearest C...C distance between the C_6F_6 and C_6H_6 molecules in the column is about 2.8 Å, close to the critical reaction distance between the benzene molecules (2.8–3.0 Å) at 298 K (Figure 1 b).^[9] This indicates a high possibility of the addition reaction between the C_6F_6 and C_6H_6 in the CHCF columns.

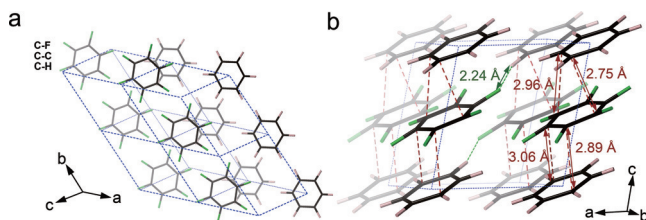


Figure 1. The crystal structure of C_6D_6 - C_6F_6 before reaction (20 GPa). Viewed perpendicular to (102) (a) and approximately along [010] (b). The black, pink, and green atoms are carbon, hydrogen (deuterium), and fluorine, respectively. This crystal structure is optimized by DFT calculations based on the structure obtained from the Rietveld refinement result of the neutron data collected at BL11 PLANET, J-PARC^[10] at 20 GPa.^[8]

Upon further compression of phase VIII using a Paris Edinburgh (PE) press, we obtained white solid samples, and their morphology varied with the applied pressure. The product recovered from 18 GPa (PE18) has an irregular morphology (see Figure S4), while that obtained from 20 GPa (PE20) shows an obviously layered structure under the scanning electron microscope (SEM; Figure 2 a). When

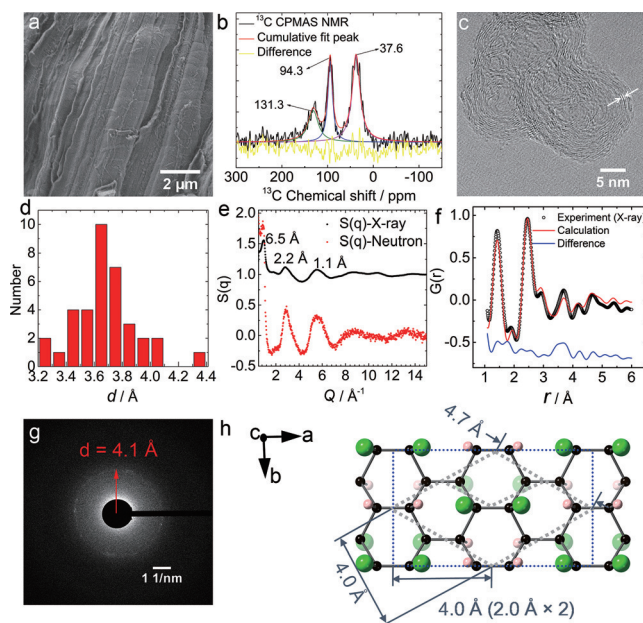


Figure 2. a) SEM images, b) ^{13}C CPMAS ssNMR spectra, and c) TEM image (200 kV) of PE20. d) The corresponding statistical results of d -spacing in c). e) The total structure factor $S(Q)$ derived from synchrotron X-ray and neutron diffraction of PE20. f) Experimental (X-ray) and calculated $G(r)$ of PE20. g) SAED pattern (120 kV TEM) of the sample PE20. The modelled PDF in Figure 2 f is derived from the proposed H-F-substituted graphane model viewed along [001] (h).

recovered from 17 GPa, the solid sample (PE17) is too limited to be analyzed, which means most of the aromatic molecules did not react and evaporated upon decompression. The energy dispersive spectroscopy (EDS) obtained from SEM shows PE20 maintains most of the fluorine atoms (see Table S2). Using solid-state nuclear magnetic resonance (ssNMR; Figure 2 b), we found three types of carbon species, $C(sp^2)$ ($\delta = 131$ ppm) and $C(sp^3)$ connected to fluorine ($F-CR_3$; $\delta = 94$ ppm) and nonfluorine atoms ($H-CR_3$; $\delta = 38$ ppm). The ratio of the peak area of the $C(sp^2)$ and $C(sp^3)$ is 1:4, which indicates $C(sp^3)$ is the dominant species. These data are consistent with the 1H -ssNMR result (see Figure S5), which is well fitted using three peaks at $\delta = 1.3$, 2.5, and 6.3 ppm, and recognized as H on $C(sp^3)$ ($H-C-R_3$), $C(sp^3)$ connected to a fluorine atom ($H-CFR_2$) and $C(sp^2)$ ($H-CR=CR_2$), respectively. Hence, the ssNMR data prove that the sample is mainly an H-F bonded sp^3 -C material.

When we measured EDS using a transmission electron microscope (TEM) of 200 kV, PE20 lost most of fluorine (see Table S2), and the corresponding image shows a curved layered structure with the interlayer d -spacing of 3.7 Å (Figure 2 c and d), consistent with that in graphite.^[11] These

data suggest that PE20 has a layered graphitic skeleton constructed from C(sp³), F, and H atoms, and lost F and H when irradiated by the 200 kV electron beam. The graphitic skeletal of PE20 is confirmed by the pair distribution function (PDF) and TEM with lower voltage. The S(Q) of neutron and X-ray PDF show bands at $d=2.2$ Å and 1.1 Å, which are ascribed to the 100 and 200 scattering, respectively, of the 2D graphitic lattice (Figure 2e). X-ray PDF ($G(r)$; Figure 2f) also shows clear features of hexagonal carbon rings at $r=1.4$, 2.5 and 2.9 Å, corresponding to the distance between 1–2, 1–3, and 1–4 positions of a hexagonal carbon ring. When using a 120 kV TEM, a diffraction ring at $d=4.1$ Å was observed in the selected area electron diffraction (SAED) pattern (Figure 2g). This d -spacing is much smaller than the interlayer spacing of graphane (4.7 Å),^[12] but close to twice of the $d(100)$ of the graphitic lattice, and hence implies a superlattice of graphene, like a 2×2 lattice (hexagonal lattice with $a=4.7$ Å and $d(100)=4.0$ Å, grey dashed line in Figure 2h) or its distorted relatives (the orthorhombic lattice in blue in Figure 2h). This arrangement probably results from the ordered bonding of H and F to the graphitic skeletal, but the details are complex and beyond the scope of this paper (see Figure S6).

All the above results indicate that PE20 has a short-range ordered hydrogenated-fluorinated graphitic structure (or hydrogenated-fluorinated graphane). The synchrotron X-ray and neutron PDF of PE20 show a clear band at $d \approx 6.5$ Å (Figure 2e), which is the typical interlayer distance of fluorinated graphite.^[13] Based on these experimental results and the reaction route mentioned later, we proposed a hydrogenated-fluorinated (H-F) graphane model for PE20 (Figure 2h) and simulated the $G(r)$ pattern, which fits the experimental data very well (Figure 2f).

The H-F graphane model for PE20 is also confirmed by the IR spectra. We optimized the proposed H-F graphane model by DFT and calculated its IR spectrum. As shown in Figure 3, among the recovered samples, PE20 featured several strong new peaks at 934, 1260, 1329, and 2924 cm⁻¹, as well as a peak at 1179 cm⁻¹ with medium intensity, and it all

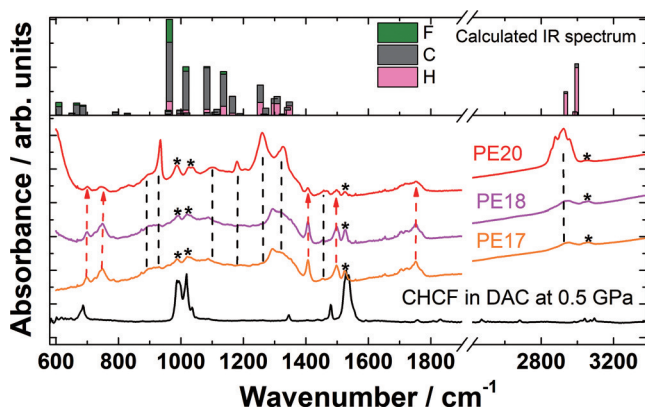


Figure 3. IR absorption spectra of PE17 (orange), PE18 (purple), PE20 (red), and CHCF starting material (black), and the calculated IR spectrum of the H-F graphane model. The assignments of the peaks in PE20 are presented in Figure S7 based on the calculated results. The assignments of the peaks in CHCF cocystal are listed in Table S3.^[8]

agrees well with the calculated IR spectrum of the H-F graphane. The peaks at 3060 cm⁻¹ [C(sp²)-H stretching], 1526 cm⁻¹ [C(sp²)-C(sp²) stretching], 1018 cm⁻¹ and 987 cm⁻¹ [C(sp²)-F stretching] are similar to the peaks of benzene or hexafluorobenzene, and are attributed to their fragments (Figure 3, marked by *). The peak at 2924 cm⁻¹ is from the C(sp³)-H stretching, which is much stronger than the peaks above 3000 cm⁻¹. This means PE20 mainly contains sp³-carbon. The contribution from F atoms is mainly located in the intermediate frequency range (933–1150 cm⁻¹), while the modes between 1160 and 1400 cm⁻¹ are dominated by the carbon and hydrogen atoms. The peak at 934 cm⁻¹ contains the C-F stretching, which is lower than that in F-graphane (C:F = 1:1).^[13a,14] This is because the C-F stretching red-shifts when fluorine atoms of F-graphane are partly substituted by hydrogen atoms.^[15] The peaks at 1179 cm⁻¹, 1260 cm⁻¹, and 1329 cm⁻¹ result from the C-H deformation and C-C stretching. The details of the assignments are summarized in Figure S7.

More importantly, in the IR spectra of PE17 and PE18, the new bands at around 699, 740, 1406 and 1753 cm⁻¹ are more intense than those in PE20 (red dashed arrows), and therefore, most likely result from intermediate products. Specifically, the peak at 699 cm⁻¹ is likely from the olefinic CH wag bands of *cis*-1,2-substitution.^[16] The peak at 740 cm⁻¹ is assigned to the olefinic CH out-of-plane vibration and is a feature of the 1,3-cyclohexadiene with a conjugated double bond, other than 1,4-cyclohexadiene.^[17] Correspondingly, the peak at 1406 cm⁻¹ is assigned to the C-H in-plane deformation related to nonfluorinated C=C bonds.^[16a,18] These features clearly confirm the 1,2-addition of benzene. In contrast, the intense band at around 1750–1756 cm⁻¹ is attributed to the C=C vibration of the nonconjugated *cis*-1,2-difluorinated olefin, thus, suggesting the occurrence of 1,4-addition for C₆F₆.^[19] All these results indicate that the [4+2] reaction happens between the C₆F₆ and C₆H₆. The decreasing intensities of these featured peaks under higher pressure indicated that the [4+2] products are related to the intermediate product, which continues to react at higher pressure.

To identify the intermediates, we extracted the soluble molecules from the samples and performed gas chromatography-mass spectrometry (GC-MS) investigations. Over 170 compounds were detected in PE20 (see Table S4), but not in the starting material. Twelve primary compounds with an abundance of more than 1% are C₁₂H₅F₅ (24.54%), C₂₄H₁₂F₁₂ (22.01%), C₁₁H₅F₅ (10.72%), C₁₂H₁₀ (9.04%), C₁₁H₅F₅ (2.40%), C₁₈H₁₀F₆ (2.11%), C₁₈F₁₈ (1.84%), C₁₈H₆F₁₂ (1.66%), C₁₀H₈ (1.42%), C₁₈H₁₂F₆ (1.28%), C₁₂H₃F₅ (1.18%), and C₁₇H₆F₁₂ (1.12%). By comparing the retention time to commercial samples and examining the National Institute of Standards and Technology/Wiley standard library, C₁₂H₅F₅, C₁₂H₁₀, and C₁₀H₈ are identified as 2,3,4,5,6-pentafluorobiphenyl, biphenyl and naphthalene, respectively (see Figure S8).

Similar results are also observed in PE17 and PE18 (see Table S5 and Table S6). Figure 4a displays the relative abundance of those representative products. C₁₂H₅F₅ is the predominant product, indicating that the 1-1' coupling reaction between C₆H₆ and C₆F₆ is a typical reaction of

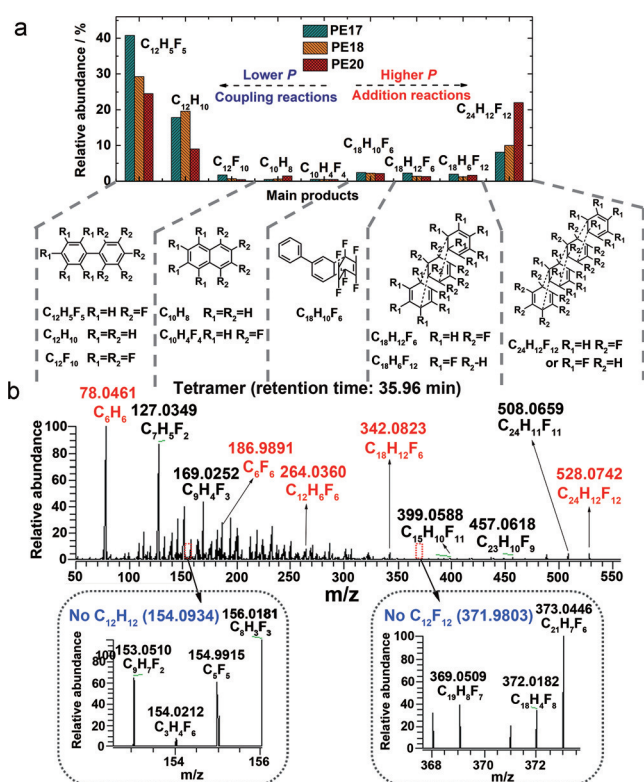
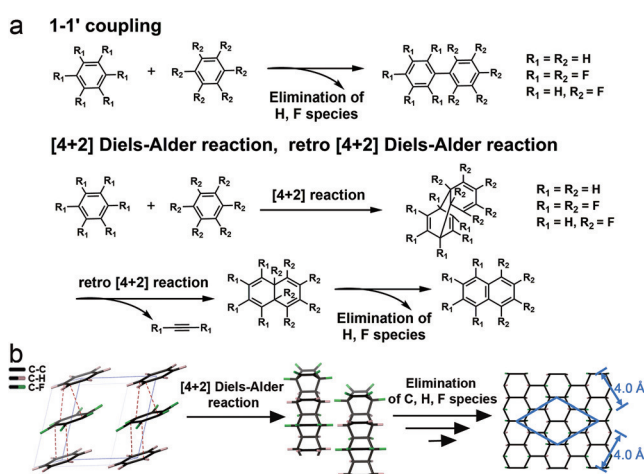


Figure 4. a) A histogram of the comparison between the relative abundance of major components in different high-pressure samples. b) The high-resolution mass spectra of the C_6H_6 - C_6F_6 tetramer at the retention time of 35.96 min in sample PE20.

CHCF under applied pressure (Scheme 1a). Considering H migrates to N in acetonitrile at a distance of 2.0 Å,^[20] the elimination of H, F species is not surprising, because the shortest intermolecular distance between H and F is 2.2 Å in phase VIII (Figure 1b). However, this does not mean that the 1-1' coupling reaction constructs the polymerized material because terphenyl ($C_{18}H_{14}$) and their fluorinated derivatives



Scheme 1. a) The selected elemental reactions of the CHCF cocrystal under high pressure. b) The proposed reaction route from CHCF cocrystal to H-F-graphane. A 2 × 2 superlattice is shown in blue line on the product.

$C_{18}(H,F)_{14}$, such as $C_{18}H_{10}F_4$, $C_{18}H_9F_5$, $C_{18}H_5F_9$, and $C_{18}H_4F_{10}$, were detected in a very small amount in all samples. In total 1.38% for PE17, 1.17% for PE18, and 1.06% for PE20. These data indicate no successive reaction is promoted by this pathway. Secondly, the IR spectra of the recovered samples significantly differ from that of the polyaryl molecules (see Figure S9).

In contrast, a series of dimers ($C_{12}H_6F_6$), trimers ($C_{18}H_6F_{12}$ and $C_{18}H_{12}F_6$), and tetramers ($C_{24}H_{12}F_{12}$) were identified, and highlights the addition between benzene and hexafluorobenzene. As shown in Figure 4a, it is notable that the $C_{24}H_{12}F_{12}$ tetramer has a much higher content when synthesized under higher pressure (PE20), and has the second highest percentage in total. Therefore, it is reasonable to infer that the addition reaction is the pathway to synthesize the CHCF polymer. In the MS of the tetramer $C_{24}H_{12}F_{12}$, the fragments $C_6H_6^+$ ($m/z = 78.0465$) and $C_6F_6^+$ ($m/z = 185.9900$) are detected, and $C_{18}H_{12}F_6^+$ and $C_{12}H_6F_6^+$ are also remarkably detected. However, no $C_{12}H_{12}^+$ and $C_{12}F_{12}^+$ ions are identified (Figure 4b). This indicates the tetramers have an alternate connection, such as C_6H_6 - C_6F_6 - C_6H_6 - C_6F_6 . Considering the [4+2] Diels-Alder reaction determined from the IR result, the PIP of C_6H_6 and C_6F_6 is most likely a process of serial [4+2] Diels-Alder reactions. We also identified a significant amount of 1,2,3,4-tetrafluoronaphthalene in the GC-MS result, and it probably comes from the following reaction process. The product of the Diels-Alder reaction undergoes a retro-Diels Alder reaction to eliminate a $C_2(H,F)_2$ molecule with subsequent elimination of two F/H species (Scheme 1a). This serial [4+2] Diels-Alder reaction of aromatics is also proposed in the literature,^[2a,5] and is consistent with the crystal structure of phase VIII in the view of topo-chemistry.

So far there is still a gap between the serial [4+2] product and H-F graphane, which is still under investigation. By comparing their structures, we arguably propose a reaction model as shown in Scheme 1b. The [4+2] polymer ribbons connect to their neighbors to form H-F graphane with a layered structure by eliminating some C, H, and F species. This model explains all the experimental results.

To conclude, we have determined the crystal structures of all the C_6H_6 - C_6F_6 cocrystal phases under high pressure and found it finally polymerized into H-F graphane with a layered structure. Several elemental reactions including the Diels-Alder, retro-Diels Alder, and 1-1' coupling reactions are discerned and the serial [4+2] Diels-Alder reaction is evidenced to be the key step of the PIP. Our investigation described the PIP process, especially the elemental reactions of CHCF for the first time, and will provide insights into the other aromatics. The formation of fluorinated graphane highlights that the PIP of the substituted aromatics is an alternative method for constructing sp^3 -hybridized carbon materials with diverse structures.

Experimental Section

Benzene (99.9%) and hexafluorobenzene (99.9%) were purchased from Sigma Aldrich and used without further purification. The C_6H_6 - C_6F_6 cocrystal (CHCF) was prepared by mixing equimolar amounts of C_6H_6 and C_6F_6 at 298 K, and storing it in a sealed bottle at

low temperature. In situ high-resolution X-ray diffraction of CHCF was conducted at Beamline 5A XRS-MS of PLS-II at Pohang Accelerator Laboratory (PAL). The neutron diffractions with a constant wavelength were collected on the Fenghuang diffractometer of China Mianyang Research Reactor (CMRR), Institute of Nuclear Physics and Chemistry, China Academy of Engineer Physics. Neutron powder diffraction measurements were made using the TOF method using the instruments at PEARL, the ISIS Neutron and Muon Facility (UK)^[21] and BL11 PLANET, J-PARC.^[10] The samples PE17, PE18, and PE20 were synthesized by a VX3 PE press equipped with double-toroid sintered diamond anvils. SEM images were recorded on a Carl Zeiss Merlin Compact Field-emission scanning electron microscope operated at 1.0 kV and the EDS result was obtained in a Carl Zeiss Merlin SEM operating at 10 kV with a system from Bruker Nano GmbH using a XFlash detector 5030. Solid ¹H and ¹³C NMR experiments were performed with a Varian-Chemagnetic Infinity 300 Nuclear Magnetic Resonance spectrometer. The TEM and SAED patterns were recorded under a bias voltage of 120 kV (ZEISS, Libra 120), and field-emission high resolution TEM were operated under a higher bias voltage of 200 kV (JEOL, JEM-2100F). High-energy PDF measurement was performed at the beamline 11-ID-C of the Advanced Photon Source (APS) at Argonne National Laboratory. The neutron PDF measurement was carried out in NOMAD, Spallation Neutron Source (SNS), Oak Ridge National Laboratory (ORNL). Mid infrared spectra were measured on a Bruker VERTEX 70v FTIR spectrometer with an IR microscope. High-resolution GC-MS measurements were performed on a Thermo Scientific™ Q Exactive™ GC hybrid quadrupole-Orbitrap mass spectrometer. Details of the in situ high-pressure XRD, neutron diffraction, the synthetic methods of the samples PE17, PE18, and PE20, ssNMR, X-ray and neutron PDF measurements, GC-MS measurement, and computational simulation methods are given in the Supporting Information.

Acknowledgements

The authors acknowledge the support of the National Natural Science Foundation of China (NSFC) (Grant Nos.: 21601007, 21771011 and 21875006). The authors also acknowledge the support from Science Challenge Project, No. TZ2016001 and the Top 1000-Talents Award. Experiments at the ISIS Neutron and Muon Source were supported by a beamtime allocation from the Science and Technology Facilities Council.^[22] Neutron diffraction experiments at J-PARC were performed through the J-PARC user programs (No. 2016A0191). The research at Oak Ridge National Lab's Spallation Neutron Source was sponsored by the Scientific User Facilities Division, Office of Basic Energy Sciences, U.S. Department of Energy (DOE). Electron microscopy experiments were conducted at the Center for Nanophase Materials Sciences, which is a DOE Office of Science User Facility. The research used resources of the Advanced Photon Source, a U.S. DOE Office of Science User Facility operated for the DOE Office of Science by Argonne National Laboratory under Contract No. DE-AC02-06CH11357. The calculations were performed on the TianheII supercomputer at the Chinese National Supercomputer Center in Guangzhou. The authors thank Dr. Joerg C. Neuefeind for his helps in neutron PDF measurement and thank Dr. Qiaoshi Zeng and Dr. Yufei Meng for their helps on the reduction of X-ray PDF data and IR measurements. X.D. thanks the support of NSFC (Grant No.: 21803033).

Conflict of interest

The authors declare no conflict of interest.

Keywords: cycloaddition · graphane · polymerization · solid-state reactions · structure determination

How to cite: *Angew. Chem. Int. Ed.* **2019**, *58*, 1468–1473
Angew. Chem. **2019**, *131*, 1482–1487

- [1] a) Z. Zeng, L. Yang, Q. Zeng, H. Lou, H. Sheng, J. Wen, D. J. Miller, Y. Meng, W. Yang, W. L. Mao, H.-k. Mao, *Nat. Commun.* **2017**, *8*, 322; b) *The properties of natural and synthetic diamond* (Ed.: J. E. Field), Academic Press, New York, **1992**.
- [2] a) T. C. Fitzgibbons, M. Guthrie, E.-s. Xu, V. H. Crespi, S. K. Davidowski, G. D. Cody, N. Alem, J. V. Badding, *Nat. Mater.* **2015**, *14*, 43–47; b) X. Li, M. Baldini, T. Wang, B. Chen, E.-s. Xu, B. Vermilyea, V. H. Crespi, R. Hoffmann, J. J. Molaison, C. A. Tulk, M. Guthrie, S. Sinogeikin, J. V. Badding, *J. Am. Chem. Soc.* **2017**, *139*, 16343–16349; c) X. Li, T. Wang, P. Duan, M. Baldini, H.-T. Huang, B. Chen, S. J. Juhl, D. Koeplinger, V. H. Crespi, K. Schmidt-Rohr, R. Hoffmann, N. Alem, M. Guthrie, X. Zhang, J. V. Badding, *J. Am. Chem. Soc.* **2018**, *140*, 4969–4972; d) M. M. Nobrega, E. Teixeira-Neto, A. B. Cairns, M. L. A. Temperini, R. Bini, *Chem. Sci.* **2018**, *9*, 254–260.
- [3] a) P. Pruzan, J. C. Chervin, M. M. Thiéry, J. P. Itié, J. M. Besson, J. P. Forgerit, M. Revault, *J. Chem. Phys.* **1990**, *92*, 6910–6915; b) F. Cansell, D. Fabre, J.-P. Petitot, *J. Chem. Phys.* **1993**, *99*, 7300–7304; c) L. Ciabini, M. Santoro, R. Bini, V. Schettino, *J. Chem. Phys.* **2002**, *117*, 2928–2935; d) B. R. Jackson, C. C. Trout, J. V. Badding, *Chem. Mater.* **2003**, *15*, 1820–1824.
- [4] M. V. Kondrin, N. A. Nikolaev, K. N. Boldyrev, Y. M. Shulga, I. P. Zibrov, V. V. Brazhkin, *CrystEngComm* **2017**, *19*, 958–966.
- [5] B. Chen, R. Hoffmann, N. W. Ashcroft, J. Badding, E. Xu, V. Crespi, *J. Am. Chem. Soc.* **2015**, *137*, 14373–14386.
- [6] A. Y. Rogachev, X. D. Wen, R. Hoffmann, *J. Am. Chem. Soc.* **2012**, *134*, 8062–8065.
- [7] a) J. S. W. Overell, G. S. Pawley, *Acta Crystallogr. Sect. B* **1982**, *38*, 1966–1972; b) J. H. Williams, J. K. Cockcroft, A. N. Fitch, *Angew. Chem. Int. Ed. Engl.* **1992**, *31*, 1655–1657; *Angew. Chem.* **1992**, *104*, 1666–1669.
- [8] Y. Wang, L. Wang, H. Zheng, K. Li, M. Andrzejewski, T. Hattori, A. Sano-Furukawa, A. Katrusiak, Y. Meng, F. Liao, F. Hong, H.-k. Mao, *J. Phys. Chem. C* **2016**, *120*, 29510–29519.
- [9] L. Ciabini, M. Santoro, F. A. Gorelli, R. Bini, V. Schettino, S. Rauegi, *Nat. Mater.* **2007**, *6*, 39–43.
- [10] T. Hattori, A. Sano-Furukawa, H. Arima, K. Komatsu, A. Yamada, Y. Inamura, T. Nakatani, Y. Seto, T. Nagai, W. Utsumi, T. Iitaka, H. Kagi, Y. Katayama, T. Inoue, T. Otomo, K. Suzuya, T. Kamiyama, M. Arai, T. Yagi, *Nucl. Instrum. Methods Phys. Res. Sect. B* **2015**, *780*, 55–67.
- [11] *Graphite and Precursors* (Ed.: P. Delhaes), CRC, Boca Raton, **2001**, ISBN 90-5699-5228-7.
- [12] a) J. Rohrer, P. Hyldgaard, *Phys. Rev. B* **2011**, *83*, 165423; b) V. E. Antonov, I. O. Bashkin, A. V. Bazhenov, B. M. Bulychev, V. K. Fedotov, T. N. Fursova, A. I. Kolesnikov, V. I. Kulakov, R. V. Lukashev, D. V. Matveev, M. K. Sakharov, Y. M. Shulga, *Carbon* **2016**, *100*, 465–473; c) X. D. Wen, R. Hoffmann, N. W. Ashcroft, *J. Am. Chem. Soc.* **2011**, *133*, 9023–9035.
- [13] a) K. Guérin, J. P. Pinheiro, M. Dubois, Z. Fawal, F. Masin, R. Yazami, A. Hamwi, *Chem. Mater.* **2004**, *16*, 1786–1792; b) V. Pishedda, S. Radescu, M. Dubois, C. Cavallari, N. Batisse, F. Balima, *Carbon* **2018**, *127*, 384–391.
- [14] a) H. Peelaers, A. D. Hernández-Nieves, O. Leenaerts, B. Partoens, F. M. Peeters, *Appl. Phys. Lett.* **2011**, *98*, 051914;

- b) Y. Liu, R. L. Vander Wal, V. N. Khabashesku, *Chem. Mater.* **2007**, *19*, 778–786; c) Y. Sato, S. Shiraishi, Z. Mazej, R. Hagiwara, Y. Ito, *Carbon* **2003**, *41*, 1971–1977.
- [15] Z. Sofer, P. Šimek, V. Mazánek, F. Šembera, Z. Janoušek, M. Pumera, *Chem. Commun.* **2015**, *51*, 5633–5636.
- [16] a) E. R. Lippincott, T. E. Kenney, *J. Am. Chem. Soc.* **1962**, *84*, 3641–3648; b) J. O. Jensen, *J. Mol. Struct. THEOCHEM* **2004**, *680*, 227–236.
- [17] a) Spectral Database for Organic Compounds, SDBS, a free site organized by National Institute of Advanced Industrial Science and Technology (AIST), Jpn, <http://sdb.sdb.aist.go.jp>; b) J. C. Berridge, A. Gilbert, G. N. Taylor, *J. Chem. Soc. Perkin Trans. I* **1980**, *38*, 2174–2178.
- [18] E. R. Blout, M. Fields, R. Karplus, *J. Am. Chem. Soc.* **1948**, *70*, 194–198.
- [19] a) N. C. Craig, E. A. Entemann, *J. Chem. Phys.* **1962**, *36*, 243–248; b) R. F. Waldron, A. C. Barefoot III, D. M. Lemal, *J. Am. Chem. Soc.* **1984**, *106*, 8301–8302; c) B. E. Roberts, G. D. Goldman, D. M. Lemal, *J. Fluorine Chem.* **1990**, *48*, 353–360.
- [20] H. Zheng, K. Li, G. D. Cody, C. A. Tulk, X. Dong, G. Gao, J. J. Molaison, Z. Liu, M. Feygenson, W. Yang, I. N. Ivanov, L. Basile, J.-C. Idrobo, M. Guthrie, H.-k. Mao, *Angew. Chem. Int. Ed.* **2016**, *55*, 12040–12044; *Angew. Chem.* **2016**, *128*, 12219–12223.
- [21] C. L. Bull, N. P. Funnell, M. G. Tucker, S. Hull, D. J. Francis, W. G. Marshall, *High Pressure Res.* **2016**, *36*, 493–511.
- [22] Y. Wang, C. Bull, K. Li, H. Zheng, Y. Wang, STFC ISIS Facility, **2017**, 1620149, <https://doi.org/10.5286/ISIS.E.84424559>.

Manuscript received: November 16, 2018

Accepted manuscript online: November 29, 2018

Version of record online: January 3, 2019